DRAFT VERSION FEBRUARY 2, 2008
Preprint typeset using LaTeX style emulateapj v. 11/12/01

INDIVIDUAL AND COLLECTIVE BEHAVIOR OF DUST PARTICLES IN A PROTOPLANETARY NEBULA

P. GARAUD, L. BARRIÈRE-FOUCHET, D. N. C. LIN
Institute of Astronomy, Madingley Road, Cambridge, CB3 0HA, UK
Centre de Recherche Astronomique de Lyon, CNRS-UMR 5574, ENS Lyon, 46 allee d'Italie, F-69364 Lyon Cedex 07 France
UCO/Lick Observatory, University of California Santa Cruz, 1156 High Street, CA 95064 Santa Cruz, USA
Draft version February 2, 2008

ABSTRACT

We study the interaction between gas and dust particles in a protoplanetary disk, comparing analytical and numerical results. We first calculate analytically the trajectories of individual particles undergoing gas drag in the disk, in the asymptotic cases of very small particles (Epstein regime) and very large particles (Stokes regime). Using a Boltzmann averaging method, we then infer their collective behavior. We compare the results of this analytical formulation against numerical computations of a large number of particles. Using successive moments of the Boltzmann equation, we derive the equivalent fluid equations for the average motion of the particles; these are intrinsically different in the Epstein and Stokes regimes. We are also able to study analytically the temporal evolution of a collection of particles with a given initial size-distribution provided collisions are ignored.

1. INTRODUCTION

In an attempt to account for the coplanar nature of the orbits of all known solar-system planets, Laplace (1796) postulated that they were formed in a common disk around the protosun. Today, the detection of protostellar disks around most young T-Tauri stars (Prosser *et al.* 1994) is a strong evidence that the Laplace nebula hypothesis is universally applicable. The recent discovery of planets around at least 10% of nearby solar-type stars (Marcy *et al.* 2000) suggests that their formation may be a robust process.

Conventional cosmogonical scenarios are based on the assumption that heavy elements in gas-phase condensed to form grains which then coagulated into planetesimals and grew into protoplanetary cores which can accrete, at least in some regions of the disk, massive gaseous envelopes around themselves (Pollack *et al.* 1996). The coexistence of gas and solid ice has been detected in some protostellar disks (Thi *et al.* 2002). In fact, protostellar disks are most conspicuous in their continuum radiation associated with the re-processing of stellar light by the grains (Adams, Lada, & Shu 1987). The apparent wavelength dependence in the thickness of the disk dust layer has been interpreted as evidence of grain growth (Throop *et al.* 2001, D'Alessio *et al.*, 2001, Clarke *et al.*, 2003) and settling (Shuping *et al.*, 2003).

The μm-to-cm continuum radiation signatures of the dust are observed to fade on the timescale of a few Myr (Beckwith, 1999, Haisch *et al.* 2001), signaling the depletion of grains in this size range. This suggests that heavy elements initially contained in this size range are either evaporated, ejected to large distance, accreted onto the host stars, or have coagulated into larger particles. The first possibility is constrained by the concurrent decline in the CO-gas (Zuckerman *et al.* 1995) whereas the last possibility is directly relevant to the process of planet formation.

Theoretical analysis suggests a very strong constraint on the growth of μm-size grains into km-size planetesimals. Indeed, the orbital evolution of the particles is determined by both the gravity of the central star and the drag of the disk gas. In the absence of turbulence, the disk gas attains a dynamical equilibrium between gravity, pressure, and centrifugal forces with zero velocity in both radial and normal-to-the-disk directions and a slightly sub-Keplerian velocity in the azimuthal direction. Particles in the disk undergo both sedimentation toward the mid-plane and inward drift in the radial direction (Whipple 1972, Weidenschilling 1977). In a minimum mass nebula (Hayashi *et al.* 1985), the resulting orbital decay timescale at 1AU (for instance) is smallest for m-size particles (Adachi *et al.* 1976), and is then less than about 10^2 yr. Unless the growth of planetesimals across this "most vulnerable size" can occur faster than their orbital decay, there would be no residual planetesimals left to provide the building blocks of planets.

One possible channel of rapid grain growth is through sedimentation into a sufficiently thin, gravitationally unstable disk (Goldreich & Ward 1973). The critical thickness for gravitational instability of such disks is less than $\sim 10^{-5}$ of their radii and the characteristic size of the resulting fragment is $\sim$ a few km. However, even a modest amount of turbulence can provide adequate stirring to prevent the sedimentation of grains into such a thin unstable layer (Weidenschilling 1984, Supulver & Lin 2000). Though turbulence is likely to occur in a magnetized disk (Balbus & Hawley, 1990) through magneto-rotational instability, this mechanism could well fail in regions of the disk where the ionization fraction is too small. In these regions only, the following alternative mechanism for turbulence has been proposed.

In a laminar disk, the sedimentation of dust toward the disk's mid-plane leads to a local concentration of massive particles; these particles entrain the gas to a near-Keplerian velocity through drag, thereby introducing a shear layer between the dust-dominated mid-plane and the rest of the disk gas (Weidenschilling & Cuzzi 1993). Such a flow pattern in the disk has the potential to cause the onset of a shearing instability (Sekiya 1998, Youdin & Shu 2002). However, the stability analysis used by these authors for such flow is based on a single-fluid approximation in which the dust particles are assumed to be well-coupled to the gas. Since the concentration of the dust particles not only causes the shear but also a stabilizing density stratification, the flow of dust and gas should be treated separately. In a companion paper (Garaud *et al.* in preparation), we will carry out a two-component stability analysis of the disk's dust layer.

Such a study is greatly simplified by the treatment of the par-

ticles as a separate fluid rather than a collection of particles. It is with this goal in mind that we now present a system of averaged equations for the evolution of a collection of dust particles in the form of moments of the Boltzmann equation. This prescription could also in principle be applied for the studies of dust particles' evolution due to coagulation, sublimation, condensation (Supulver & Lin 2000) and under their interaction with embedded planets (Wyatt *et al.* 1999) and stellar radiation (Takeuchi & Artymowicz 2001, Klahr & Lin 2001, Takeuchi & Lin 2002).

For the present calculation, we assume the particles are collisionless and indestructible spheres in a gaseous laminar disk with no embedded planets and negligible stellar radiation. In this paper, we also neglect the feedback of the particles' drag on the motion of the gas. In §2, we recall the general gas drag laws and their effects on particle trajectories in a protoplanetary accretion disk. In §3, and §4 we solve for individual particles' orbits, and derive the complementary set of dynamical equations for a collection of particles in the form of low-order moments of the Boltzmann equation (Boltzmann, 1872). In §3, we focus only on small particles, which have sizes smaller than the mean-free-path of the gas molecules, whereas in §4, we develop analogous equations for particles with sizes larger than the mean-free-path of gas. These initial calculations are purely analytic; in order to perform them, we need to assume separation of the radial and normal-to-the-disk variables, as well as a constant background gas density. In §5, we check the validity of these assumptions with a complete numerical calculation of the particles' orbits in a simple-to-use model for the gas nebula. We compare both the results for individual orbits and for the moments (typically, the average velocity and average velocity dispersion) obtained from the Boltzmann averaging procedure. We also consider the spatial and temporal evolution of a given size-distribution of particles in §6 and show that particles with a narrow selected size-range sediment most rapidly toward the mid-plane. Finally in §7, we summarize our results and discuss their implications.

2. GAS DRAG LAWS AND PARTICLE MOTION

In this section, we briefly recall the effect of gas drag and gravitational forces on individual particle trajectories.

2.1. *Drag force description*

In dust-particle number-density regimes where particle collisions are negligible, the trajectory of a particle is given by

$$\mathbf{r}'' = -\nabla\Phi - \frac{1}{m_\mathrm{p}}\mathbf{F}_\mathrm{d}\,, \tag{1}$$

where q' denote derivatives of q with respect to time, $\mathbf{r}$ is the position vector of the particle, Φ is the externally imposed gravitational potential, m_p is the mass of the particle and $\mathbf{F}_\mathrm{d}$ is the drag force between the particle and the gas. The amplitude of the drag force depends on the size of the particle s compared to the mean free path of the gas λ and one typically distinguishes two regimes, $s \ll \lambda$ (Epstein regime) and $s \gg \lambda$ (Stokes regime).

In the small particle limit, *i.e.* the Epstein regime, the drag is caused by the thermal agitation of the gas and is proportional to the velocity of the particle relative to the gas:

$$\mathbf{F}_\mathrm{d} = m_\mathrm{p}\frac{\rho}{\rho_\mathrm{s}}\frac{c}{s}(\dot{\mathbf{r}}-\mathbf{v}_\mathrm{g}) \text{ when } s \ll \lambda\,, \tag{2}$$

where $\mathbf{v}_\mathrm{g}$ is the gas velocity, ρ is the local density of the gas, c is the local sound speed and ρ_s is the solid (i.e. internal) density of the particle. In a standard solar nebula, this formula is typically valid up to decimeter-sized particles at 1 AU.

In the other limit, large particles see the gas as a fluid, and experience a drag force through the laminar or turbulent wake that they create as they move through the gas. This is the Stokes regime. Whipple (1972) reported that the drag force on a sphere is

$$\mathbf{F}_\mathrm{d} = m_\mathrm{p}\frac{\rho}{\rho_\mathrm{s}}\frac{C(Re)}{s}|\Delta\mathbf{v}|(\dot{\mathbf{r}}-\mathbf{v}_\mathrm{g}) \text{ when } s \gg \lambda\,, \tag{3}$$

where $|\Delta\mathbf{v}|$ is the norm of $\dot{\mathbf{r}}-\mathbf{v}_\mathrm{g}$ and Re is the particle Reynolds number of the flow ($Re = 2s|\Delta\mathbf{v}|/\nu$ where $\nu = \lambda c/3$ is the molecular viscosity of the gas). Experimental results suggest that the drag coefficient $C(Re)$ varies like

$$\begin{aligned} C &= 9Re^{-1} \text{ for } Re \le 1\,,\\ C &= 9Re^{-0.6} \text{ for } 1 \le Re \le 800\,,\\ C &= 0.165 \text{ for } 800 \le Re\,. \end{aligned} \tag{4}$$

This prescription ensures a smooth transition between the Epstein regime and the Stokes regime for intermediate particle sizes ($s \simeq \lambda$). Note that in the Stokes regime (for $Re \to \infty$), the amplitude of the drag force depends on the total velocity of the particle with respect to the gas, and not simply its component parallel to the particle's velocity. This expresses the fact that a strong wake caused by the particles motion in one direction also affects even the slightest motion in another perpendicular direction.

2.2. *Separation of vertical and radial motions*

As particles undergo gas drag, they lose angular momentum which causes them to drift slowly inwards. For particles strongly coupled to the gas (i.e. very small particles), this drift is slowed down by the support provided by the gas pressure itself. For weakly coupled particles (i.e. very large particles), the angular-momentum loss is very small and the drift is equally slow (see the next section). There exists an intermediate regime, however, where orbital decay can occur very rapidly. Weidenschilling (1977) carried out a first quantitative study of the effect of the gas drag on particles of various sizes, and determined the inward drift velocity as a function of particle size. He found that the maximal drift occurs for particles for which the typical stopping timescale $t_s = |(\mathbf{r}'-\mathbf{v}_\mathrm{g})|/|\mathbf{F}_\mathrm{d}|$ is of order of the orbital timescale Ω_K^{-1}, and decays very quickly for particles much larger, or much smaller than that. As a result, unless the particle is of intermediate size, there will be a marked separation between the dynamical timescale and the orbital decay timescale.

Moreover, there is also a marked separation between radial and vertical length scales; indeed, numerical integration of the orbits of particles in a gaseous disk shows that the typical radial drift velocity is of the same order (in the case of small particles) or much smaller (in the case of large particles) than the vertical settling velocity (see Section 5.2). Hence in a thin disk the particles settle to the mid-plane with very little radial excursion, then undergo radial decay within a very thin dust layer. For this reason it is justified to assume that the vertical motion of particles is more or less independent of their radial motion (although not of their radial *position*), and that their radial motion occurs mostly at $z = 0$. Since Weidenschilling (1977) has already derived an analytical description of the particles motion in the radial direction, we shall concentrate on the problem of vertical settling. A short derivation of the case of radial and azimuthal motion of the particles in a gas disk is presented in the Appendix for completeness.

3. THE COLLECTIVE EVOLUTION OF SMALL PARTICLES

3.1. *Vertical motion of small particles in the Epstein regime*

From the previous sections, we infer the vertical equation of motion of a small dust-particle in the Epstein regime:

$$z'' = -\frac{\partial\Phi}{\partial z} - \frac{\rho}{\rho_s}\frac{c}{s}z' \,, \tag{5}$$

where z is the height above the disk. In a central potential, the gravitational force close to the mid-plane can be rewritten as $-\Omega_K^2(r)z$ where $\Omega_K(r)$ is the Keplerian angular velocity at the radius considered. We re-normalize the time variable to the orbital timescale $t_o = \Omega_K^{-1}$ at the radial position considered, and the distances to Astronomical Units (AU); we deduce the non-dimensional equation

$$\ddot{z} = -z - \mu\dot{z} \,, \tag{6}$$

where $\mu = \Omega_K^{-1}(r)(\rho(r)/\rho_s)(c(r)/s)$. In terms of this normalization, the magnitude of μ in this regime is typically much larger than unity, which means that the stopping time $1/\mu$ is much smaller than the orbital time. The solution to equation (6) is straightforward, and the trajectory of a particle initially positioned at height z_i with initial velocity w_i is

$$z_p(\mu,t;z_i,w_i) = \frac{1}{2}\left[\left(z_i + \frac{2w_i+\mu z_i}{\sqrt{\mu^2-4}}\right)\exp\left(\frac{-\mu+\sqrt{\mu^2-4}}{2}t\right) + \left(z_i - \frac{2w_i+\mu z_i}{\sqrt{\mu^2-4}}\right)\exp\left(\frac{-\mu-\sqrt{\mu^2-4}}{2}t\right)\right] . \tag{7}$$

Note that for $\mu \gg 1$ this expression simplifies to

$$z_p(\mu,t;z_i,w_i) = \left(z_i + \frac{w_i}{\mu}\right)e^{-t/\mu} - \frac{w_i}{\mu}e^{-\mu t} \,. \tag{8}$$

The second term of this expression describes the rapid deceleration of the particle by the gas drag, the first represents a slow settling toward the mid-plane. Let us recast this equation into

$$z_p(\mu,t;z_i,w_i) = \alpha(\mu,t)z_i + \beta(\mu,t)w_i \,, \tag{9}$$

which defines the functions α and β uniquely. The instantaneous vertical velocity of these particles is then given by

$$w_p(\mu,t;z_i,w_i) = \dot{z}_p = \dot{\alpha}z_i + \dot{\beta}w_i \,. \tag{10}$$

Note that for $\mu \simeq 1$ (which describes the intermediate parameter range between the Epstein regime and the Stokes regime) the particle motion contains an oscillatory component decaying exponentially on timescale $\mu/2$.

3.2. *Boltzmann description and continuum equations*

Given a set of particles at initial positions z_i and with initial velocities w_i, the Boltzmann distribution function of these particles is

$$f(z,w,t) = \sum_i m_i \delta(z - z_p(\mu,t;z_i,w_i))\delta(w - w_p(\mu,t;z_i,w_i)) \,. \tag{11}$$

One can also take the continuum limit of this description in the case of a very large number of particles:

$$f(z,w,t) = \int dz_i \int dw_i \;\; \rho_i(z_i)g(w_i,z_i)\delta(z - z_p(\mu,t;z_i,w_i)) \cdot\delta(w - w_p(\mu,t;z_i,w_i)) \,, \tag{12}$$

where ρ_i is the initial particle density distribution, and g is the initial velocity distribution of particles. The freedom in the relative choices of the initial distribution functions ρ_i and g is lifted by requiring that for all z_i

$$\int dw_i \; g(w_i,z_i) = 1 \,. \tag{13}$$

The mass density of the particles is obtained by integrating f over all possible velocities:

$$\rho_p(z,t) = \int dw f(z,w,t) = \int dz_i \int dw_i \rho_i(z_i)g(w_i,z_i)\delta(z - z_p(\mu,t;z_i,w_i)) \,. \tag{14}$$

Substitution of the equations for the particle trajectories into (14) and integration over all possible initial positions yields

$$\rho_p(z,t) = \frac{1}{\alpha}\int dw_i \rho_i \left(\frac{z-\beta w_i}{\alpha}\right) g\left(w_i, \frac{z-\beta w_i}{\alpha}\right) \,. \tag{15}$$

The first moment of the Boltzmann function is the average vertical velocity:

$$\rho_p(z,t)\overline{w} = \int dw w f(z,w,t) = \int dz_i \int dw_i \rho_i(z_i)g(w_i,z_i)w_p\delta(z - z_p(\mu,t;z_i,w_i)) \,. \tag{16}$$

The same manipulations yield

$$\rho_p\overline{w} = \int \frac{dw_i}{\alpha}\rho_i \left(\frac{z-\beta w_i}{\alpha}\right) g\left(w_i, \frac{z-\beta w_i}{\alpha}\right)\left(\dot{\alpha}\frac{z-\beta w_i}{\alpha} + \dot{\beta}w_i\right) \tag{17}$$

Let us assume for a short while that the distribution of the initial velocities is independent of height above the mid-plane. Then we can verify easily that the quantities determined above in equations (15) and (17) satisfy the standard continuity equation

$$\frac{\partial\rho_p}{\partial t} + \frac{\partial}{\partial z}(\rho_p\overline{w}) = 0 \,, \tag{18}$$

regardless of the form of the "trajectory functions" α and β.

However, the original collisionless Boltzmann equation (Boltzmann, 1872) describes the evolution of the distribution function f in phase space through

$$\frac{\partial f}{\partial t} + w\frac{\partial f}{\partial z} + \dot{w}\frac{\partial f}{\partial w} = \Gamma \,, \tag{19}$$

where Γ is a collision term that reproduces the interaction of the particles with themselves and with the surrounding medium. If we integrate the Boltzmann equation with respect to the velocity space, we get

$$\frac{\partial\rho_p}{\partial t} + \frac{\partial}{\partial z}(\rho_p\overline{w}) + \int dw\dot{w}\frac{\partial f}{\partial w} = \int \Gamma dw \,. \tag{20}$$

Substitution of the equation of motion equation (6) into the last term of the left-hand-side provides an expression for the interaction term Γ as a condition for the mass continuity equation to be satisfied:

$$\Gamma = \mu f \,. \tag{21}$$

This result can be generalized in the case where g depends on z_i.

Subtracting the mass continuity equation from the first moment of the Boltzmann equation reveals the importance of the particle velocity correlations $\overline{w^2}$

$$\rho_p\frac{\partial\overline{w}}{\partial t} + \rho_p\overline{w}\frac{\partial\overline{w}}{\partial z} = -\rho_p\frac{\partial\Phi}{\partial z} - \mu\rho_p\overline{w} - \frac{\partial}{\partial z}(\rho_p\sigma^2) \,, \tag{22}$$

where $\sigma^2 = \overline{w^2} - \overline{w}^2$ represents the particles' velocity dispersion function. This equation is very similar to that of a standard fluid, with the following caveats: (i) it contains an explicit drag term in the form of $-\mu\overline{w}$, and (ii) the very last term, which usually represents the pressure term in a standard fluid[1], must be written explicitly as a function of known quantities. We expect this term to be null in the case of collisionless particles with negligible relative velocity with respect to the gas; in order to double check this conjecture, we now evaluate σ^2 explicitly.

Let us first evaluate $\overline{w^2}$:

$$\rho_p \overline{w^2} = \int \frac{dw_i}{\alpha} \rho_i \left(\frac{z - \beta w_i}{\alpha} \right) g \left(w_i, \frac{z - \beta w_i}{\alpha} \right) \left(\dot{\alpha} \frac{z - \beta w_i}{\alpha} + \dot{\beta} w_i \right)^2 \quad (23)$$

The behavior of σ^2 at short times (i.e. for times shorter than the stopping time $t_s = 1/\mu$) is difficult to extract analytically while keeping the functions ρ_i and g unprescribed. However, for large μ and large times one can simplify the expressions for the functions α and β to

$$\alpha = \exp(-t/\mu) + O(\exp(-\mu t)) ,$$
$$\beta = \frac{1}{\mu} \left(\exp(-t/\mu) - \exp(-\mu t) \right) . \quad (24)$$

In that case, the expressions for the first and second velocity moments simplify largely to

$$\overline{w} = -\frac{z}{\mu} + O(\exp(-\mu t)) ,$$
$$\overline{w^2} = \frac{z^2}{\mu^2} + O(\exp(-\mu t)) , \quad (25)$$

and one can show that provided g is an even function of velocity

$$\sigma^2 = O(\exp(-2\mu t)) . \quad (26)$$

This result is expected: any initial velocity dispersion is quickly damped out by the surrounding gas on the short stopping timescale t_s. Note that in the case where ρ_i and g are uniformly distributed, this expression is also valid for very short times. The long-term evolution of the collection of particles becomes a slow collective settling, on a timescale μ. Therefore, in the Epstein case, one can approximate the particles as a fluid with a linear drag force and zero pressure.

4. THE COLLECTIVE EVOLUTION OF LARGE PARTICLES

The main drag effect of the gas on a large particle occurs through the formation of a wake behind the particle. If the velocity of the particle relative to the gas is small enough, the wake is laminar and the drag force is a linear function of the relative velocity. In that case, the particle trajectory is actually the same as that obtained in the case of the Epstein regime, and the results of the previous section apply. However, as the relative velocity between the particle and the gas increases, the wake becomes turbulent and the amplitude of the drag force becomes a power law of the particle's Reynolds number.

As a result, though the component of the drag force in any direction is still proportional to the relative velocities of the particle and the gas in that same direction, its amplitude also depends on the total relative velocity of the particle with respect to the fluid. Hence the vertical component of the drag force is:

$$\mathbf{F}_d \cdot \hat{\mathbf{e}}_z = -m_p \frac{\rho(r)}{\rho_s} \frac{C(Re)}{s} \sqrt{r'^2 + z'^2 + (r\theta' - v_g)^2} z' , \quad (27)$$

if one assume the only important component of the gas velocity is in the azimuthal direction. This formula can in principle be used only in conjunction with a complete evaluation of the particle's orbit. However, one can assume that the largest typical contrasts in velocity between particle and gas occurs in the vertical direction, where the particles oscillate across the mid-plane with an epicyclic frequency whereas the gas is more-or-less stationary (so that $z'^2 \gg (r\theta' - v_g)^2$ and $z'^2 \gg r'^2$). In that case, the expression for the vertical component of the drag force reduces to

$$\mathbf{F}_d \cdot \hat{\mathbf{e}}_z = -m_p \frac{\rho(r)}{\rho_s} \frac{C(Re)}{s} |z'| z' . \quad (28)$$

Note that since the typical velocity of the particles across the mid-plane is of order of $\Delta\Omega_K$ where Δ is the typical height of particles above the disk, the asymptotic Stokes regime occurs for particles of size

$$\frac{s}{\lambda} = \frac{Re_c}{6} \frac{r}{\Delta} \frac{v_K}{c} , \quad (29)$$

where $Re_c = 800$. This condition corresponds for example to 10 m size particles at $r = 1$ AU and $\Delta = 1/10$th of the disk scale height in a standard solar nebula.

4.1. *Particles' trajectories*

Using the same normalizations as in the Epstein regime, the particle's vertical equation of motion can then be written as

$$\ddot{z} = -z - \mu |\dot{z}| \dot{z} , \quad (30)$$

where $\mu = C(Re)(R/s)(\rho/\rho_s)$ and $R = 1$ AU. In the asymptotic Stokes regime, $C(Re)$ is simply a constant, and μ is typically of order of unity, or smaller.

This equation can be solved exactly through the introduction of the quantity $w = \dot{z}$. On the positive branch (when $w > 0$) and negative branch ($w < 0$) the solutions are, respectively,

$$w_+^2 = A \exp(-2\mu z) - \frac{z}{\mu} + \frac{1}{2\mu^2} ,$$
$$w_-^2 = B \exp(2\mu z) + \frac{z}{\mu} + \frac{1}{2\mu^2} . \quad (31)$$

As the particle oscillates about the mid-plane, it follows one branch or the other. The constants A and B are determined by matching the first branch to the boundary conditions and the successive alternative ones to each other at the turning point (i.e. when $w = 0$). For instance, the trajectory of a particle starting from rest at $z = z_0$ above the mid-plane satisfies the equation

$$w_-^2 = \dot{z}^2 = \left(-\frac{z_0}{\mu} - \frac{1}{2\mu^2} \right) \exp(2\mu z - 2\mu z_0) + \frac{z}{\mu} + \frac{1}{2\mu^2} . \quad (32)$$

It accelerates toward the mid-plane, then decelerates on the other side until it reaches a turning point z_1 which satisfies

$$0 = \left(-\frac{z_0}{\mu} - \frac{1}{2\mu^2}) \right) \exp(2\mu z_1 - 2\mu z_0) + \frac{z_1}{\mu} + \frac{1}{2\mu^2} . \quad (33)$$

These solutions indicate the existence of two regimes. When the initial height z_0 is much larger than the scale height $1/\mu$ the turning point z_1 is roughly equal to $1/2\mu$ regardless of the height from which it originated. This pattern corresponds to a rapid stopping phase, when the particle quickly drops toward the mid-plane. When the amplitude of z_0 is reduced much below $1/\mu$, the turning point z_1 is roughly equal to $-z_0$, which corresponds to the oscillatory phase, when the particle follows an epicyclic motion about the mid-plane with a slowly decaying amplitude.

[1] this term is related to thermal elastic collisions of the gas particles in a standard fluid, and tends to depend only on the local density and temperature of the fluid

4.2. *The very rapid stopping phase*

The stopping phase corresponds to the limit where z is much larger than the scale height $1/\mu$. Note that this situation may not always occur since in the Stokes regime, $\mu \leq 1$. This condition corresponds to particles which start at a considerable distance above or below the disk itself. Nonetheless, in this case the solutions simplify to:

$$w_-^2 \simeq \frac{z}{\mu} \equiv \dot{z} \simeq -\frac{z^{1/2}}{\mu^{1/2}} , \tag{34}$$

(for the downward branch) and this differential equation can easily be solved with

$$z_\mathrm{p}(t) = \left(z_0^{1/2} - \frac{t}{2\mu^{1/2}} \right)^2 . \tag{35}$$

Note that the particle velocity in that case varies linearly with time:

$$w_\mathrm{p}(t) = -2 \left(\frac{z_0}{\mu} \right)^{1/2} + \frac{t}{2\mu} , \tag{36}$$

so that the typical duration of the settling phase is $t_s = 2\mu^{1/2} z_0^{1/2}$. Finally, we also note that for a particle starting from z_0 above the disk, for example, the lower turning point is more or less independent of z_0 and is roughly equal to $z_1 = -1/2\mu$.

4.3. *The slowly decaying oscillating phase*

The oscillating phase corresponds to the limit $z \ll 1/\mu$. In that case, the equation for the trajectory of the particle (in the downward branch, for example) simplifies to

$$w_-^2 = \dot{z}^2 = 2z_0(z_0 - z) - (1 + 2\mu z_0)(z_0 - z)^2 . \tag{37}$$

This first order differential equation can be solved with conventional substitutions to yield

$$z_\mathrm{p}(t) = z_0 - \frac{z_0}{1 + 2\mu z_0} \left[1 - \cos\left((1 + 2\mu z_0)^{1/2} t \right) \right] . \tag{38}$$

The lower turning point is then simply

$$z_1 = z_0 - \frac{2z_0}{1 + 2\mu z_0} . \tag{39}$$

Starting from that point, the upward branch is then obtained through a similar analysis and becomes

$$z_\mathrm{p}(t) = z_1 - \frac{z_1}{1 - 2\mu z_1} \left[1 - \cos\left((1 - 2\mu z_1)^{1/2} t \right) \right] . \tag{40}$$

The following upper turning point is z_2 such that

$$z_2 = z_1 - \frac{2z_1}{1 - 2\mu z_1} . \tag{41}$$

These equations show that the amplitude $\gamma(t)$ of the oscillation slowly decays with time, and can be approximated by

$$\gamma(t) \simeq \frac{3\pi}{4\mu t + K} , \tag{42}$$

where K is a constant which is determined in such a way as to satisfy the initial conditions. If the particle is released from rest from $z = z_0$ at $t = 0$ (with $z_0 \ll 1/\mu$), $K = 3\pi/z_0$. Moreover the frequency of the oscillation also varies with time, and converges to the epicyclic frequency.

To recapitulate briefly, we find that after a brief stopping phase on a timescale proportional to $\mu^{1/2}$, the particle oscillates around the mid-plane with frequency which is close to the epicyclic frequency, and with an amplitude that decays slowly in time roughly as given by equation (42). These solutions are illustrated in Figure 1.

4.4. *Continuum equations in the Stokes regime*

The true particle trajectory in the asymptotic Stokes regime cannot be expressed analytically in any simple way. As in the Epstein case, we will only look at long-term behavior. In that case, we can approximate the trajectory of a particle by

$$z_\mathrm{p}(t, \mu; K_i, \varphi_i) = \gamma(\mu, t; K_i) \cos(t + \varphi_i) , \tag{43}$$

where K_i and φ_i are complicated functions of the initial position and velocity of the particle. For simplicity, we will consider the asymptotic limit for times $4\mu t >> K_i$. In this limit, equation (43) with $\gamma = 3\pi/4\mu t$ is a good approximation, since the amplitude of the particle trajectory becomes independent of the point of release (see Fig. 1). Let us also assume for the purpose of this work that the phase simply has a given distribution function $g(\varphi)$ so that Boltzmann function for the Stokes regime is

$$\begin{aligned} f(z, w, t) &= \int \mathrm{d}z_0 \rho_i(z_0) \int_0^{2\pi} \mathrm{d}\varphi g(\varphi) \delta(z - z_\mathrm{p}(\mu, t; \varphi)) \\ &= \Sigma_\mathrm{p} \int \mathrm{d}\varphi g(\varphi) \delta(z - z_\mathrm{p}(\mu, t; \varphi)) , \end{aligned} \tag{44}$$

where Σ_p is the column density of particles, and the normalization of g is chosen such that $\int_0^{2\pi} \mathrm{d}\varphi g(\varphi) = 1$. The function g is periodic with period 2π but the initial distribution of particles can be described with $0 \leq \varphi \leq 2\pi$. Using the well-known relation

$$\delta(h(x)) = \sum_i \delta(x - x_i) \left| \frac{\mathrm{d}h}{\mathrm{d}x}(x = x_i) \right|^{-1} \text{ where } h(x_i) = 0 , \tag{45}$$

we can determine the particle mass density profile,

$$\begin{aligned} \rho_\mathrm{p}(z, t) = \; & \frac{\Sigma_\mathrm{p}}{\gamma} \mathcal{H}(\gamma - |z|) \left(1 - \frac{z^2}{\gamma^2} \right)^{-1/2} \\ & \cdot \left[g\left(\cos^{-1}(z/\gamma) - t \right) + g\left(-\cos^{-1}(z/\gamma) - t \right) \right] , \end{aligned} \tag{46}$$

where $\mathcal{H}$ is a Heaviside function and the function $\cos^{-1}$ takes values in the interval $[0, \pi]$.

As in the Epstein case, we can compare the fluid equation for mass conservation to the first moment of the Boltzmann equation and obtain an expression for the collision term in the Stokes regime:

$$\Gamma = 2\mu |w| f . \tag{47}$$

Similar operations with the second moment of the Boltzmann equation yields the equivalent of the fluid equation of motion,

$$\rho_\mathrm{p} \frac{\partial \overline{w}}{\partial t} + \rho_\mathrm{p} \overline{w} \frac{\partial \overline{w}}{\partial z} = -\rho_\mathrm{p} \frac{\partial \Phi}{\partial z} - \int \mu f |w| w \, \mathrm{d}w - \frac{\partial}{\partial z} (\rho_\mathrm{p} \sigma^2) . \tag{48}$$

It is extremely tempting to write the drag term as

$$\int \mu f |w| w \, \mathrm{d}w = \mu \rho_\mathrm{p} |\overline{w}| \overline{w} . \tag{49}$$

However, a proper evaluation of the left-hand-side integral shows that this cannot be done formally, and the complete expression for the drag force term should be kept. From equations (43) and (44),

$$\begin{aligned} \int f |w| w \, \mathrm{d}w = \; & \frac{\Sigma_\mathrm{p}}{\gamma} \left(1 - \frac{z^2}{\gamma^2} \right)^{-1/2} \mathcal{H}(\gamma - |z|) \\ & \cdot \left[g(\cos^{-1}(z/\delta) - t) \left(\frac{z\dot{\gamma}}{\gamma} - \gamma \sqrt{1 - \frac{z^2}{\gamma^2}} \right) \left| \frac{z\dot{\gamma}}{\gamma} - \gamma \sqrt{1 - \frac{z^2}{\gamma^2}} \right| \right. \\ & \left. + \, g(-\cos^{-1}(z/\delta) - t) \left(\frac{z\dot{\gamma}}{\gamma} + \gamma \sqrt{1 - \frac{z^2}{\gamma^2}} \right) \left| \frac{z\dot{\gamma}}{\gamma} + \gamma \sqrt{1 - \frac{z^2}{\gamma^2}} \right| \right] . \end{aligned} \tag{50}$$

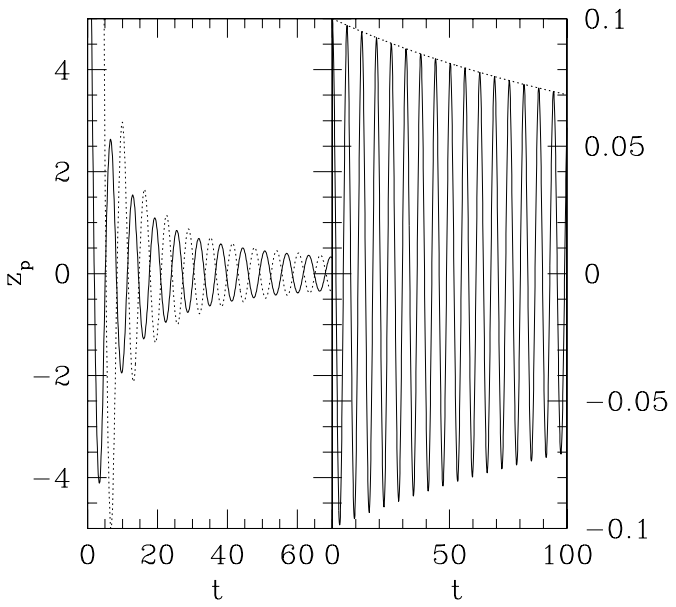

FIG. 1.— *Left panel:* Trajectories of two particles as integrated numerically from the differential equation (30). The particles were released from rest from heights $10r$ (solid line) and $100r$ (dotted line), in the case where $\mu = 0.1$. Note that the first lower turning point is always located around $-1/2\mu$ and that the oscillation amplitude is independent of the point of release in the following oscillating period. However, depending on the initial condition, a phase difference can exist between two trajectories. *Right panel:* Trajectories of a particle released from rest from height 0.1 above the disk, with $\mu = 0.1$. The particle oscillates around the mid-plane with an amplitude that decreases algebraically with time; the dotted line was drawn according to the amplitude given by equation (42).

In the case where g is uniformly distributed, this expression reduces to

$$\int f|w|w\mathrm{d}w = \frac{\rho_\mathrm{p}}{2}\left[\left(\frac{z\dot\gamma}{\gamma}-\gamma\sqrt{1-\frac{z^2}{\gamma^2}}\right)\left|\frac{z\dot\gamma}{\gamma}-\gamma\sqrt{1-\frac{z^2}{\gamma^2}}\right| + \left(\frac{z\dot\gamma}{\gamma}+\gamma\sqrt{1-\frac{z^2}{\gamma^2}}\right)\left|\frac{z\dot\gamma}{\gamma}+\gamma\sqrt{1-\frac{z^2}{\gamma^2}}\right|\right] , \quad (51)$$

whereas the simpler expression $\rho_\mathrm{p}|\overline{w}|\overline{w}$ in equation (49), which is rewritten $\rho_\mathrm{p}(z\dot\gamma/\gamma)|z\dot\gamma/\gamma|$ in that case, would be wrongly applied.

As before, we are interested in evaluating the velocity dispersion σ^2. We need to calculate

$$\frac{\rho_\mathrm{p}\overline{w}}{\Sigma_\mathrm{p}} = \int_0^{2\pi}\mathrm{d}\varphi g(\varphi)\delta(z-\gamma\cos(\varphi+t))\,(\dot\gamma\cos(t+\varphi)-\gamma\sin(t+\varphi)) \ . \quad (52)$$

In the asymptotic limit

$$\frac{\rho_\mathrm{p}\overline{w}}{\Sigma_\mathrm{p}} = \frac{\mathcal{H}(\gamma-|z|)}{\gamma}\left[\left(\frac{\dot\gamma}{\gamma}\left(1-\frac{z^2}{\gamma^2}\right)^{-1/2}z-\gamma\right)g\left(\cos^{-1}(z/\delta)-t\right) + \left(\frac{\dot\gamma}{\gamma}\left(1-\frac{z^2}{\gamma^2}\right)^{-1/2}z+\gamma\right)g\left(-\cos^{-1}(z/\delta)-t\right)\right] \quad (53)$$

$$= \frac{\rho_\mathrm{p}}{\Sigma_\mathrm{p}}\frac{\dot\gamma}{\gamma}z - \mathcal{H}(\gamma-|z|) \cdot\left[g\left(\cos^{-1}(z/\delta)-t\right)-g\left(-\cos^{-1}(z/\delta)-t\right)\right] \ .$$

Similarly, one can show that

$$\rho_\mathrm{p}\overline{ww} = \Sigma_\mathrm{p}\int_0^{2\pi}\mathrm{d}\varphi\ \ g(\varphi)\delta(z-\gamma\cos(\varphi+t)) \cdot(\dot\gamma\cos(t+\varphi)-\gamma\sin(t+\varphi))^2 \ , \quad (54)$$

so that in the asymptotic limit

$$\rho_\mathrm{p}\overline{ww} = \rho_\mathrm{p}\left(\frac{z^2\dot\gamma^2}{\gamma^2}+(\gamma^2-z^2)\right)-2\Sigma_\mathrm{p}\mathcal{H}(\gamma-|z|)\dot\gamma z \cdot\left[g(\cos^{-1}(z/\delta)-t)-g(-\cos^{-1}(z/\delta)-t)\right] \ . \quad (55)$$

In the case where the initial distribution function g is uniform, we can simplify these expressions greatly and show that for $|z| \le \gamma$ (which corresponds to the thickness of the dust layer) then

$$\sigma^2 = (\gamma^2-z^2)\mathcal{H}(\gamma-|z|) \ . \quad (56)$$

This expression means that within the dust disk, the particle velocity dispersion remains important at all times. The velocity dispersion mimics the effect of a pressure term which effectively slows down the settling. In this simplified case where $g(\varphi)$ was taken to be a uniform distribution, it is actually possible to relate σ to intrinsic large-scale properties of the system. However in the more general case where $g(\varphi)$ is not a uniform distribution there exists no simple relationship between σ^2 and the local density of the gas as there would normally be in a standard fluid. Instead, this mock-pressure terms would depend in a complicated manner on the initial configurations of the particles in phase-space. This prevents any further progress, at this stage, in the use of a fluid description for these large particles.

5. NUMERICAL CALCULATIONS

With this simplified analytical approach, we have explored what effects the gas drag may have on particles of various sizes. Three principal approximations were performed:

- we neglected the radial motion of the particles, and therefore implicitly assumed that it is possible to perform a separation of the variables and of the equations of motion into individual components;

- we neglected the vertical variation of μ and used a simplified expression for the gravity,
- we neglected the contribution of the azimuthal motion of the particles through the gas in the calculation of the gas drag in the Stokes regime. This approximation effectively underestimates the gas drag.

In order to check the validity of these approximations, we begin by integrating the orbits of particles in a realistic gaseous protoplanetary nebula, with the complete expression for the gas drag force. We compare them to the corresponding analytical expressions. We then release various single-size sets of 10,000 particles in the disk from a small region and follow their evolution in time. At a given time t we then perform the Boltzmann averaging procedure and compare the results with those obtained in Sections 3 and 4.

5.1. *Numerical Integration: method and model parameters*

The equation of motion of a particle in a gaseous accretion disk is given by equation (1). Expanding this equation into its components in a cylindrical coordinate system (r,θ,z) yields

$$\begin{aligned} r'' &= r\theta'^2 - \frac{GMr}{(r^2+z^2)^{3/2}} - \frac{\mathbf{F}_\mathrm{d}}{m_\mathrm{p}}\cdot\hat{\mathbf{e}}_r \,, \\ \theta'' &= -2\frac{r'}{r}\theta' - \frac{\mathbf{F}_\mathrm{d}}{m_\mathrm{p}}\cdot\hat{\mathbf{e}}_\theta \,, \\ z'' &= -\frac{GMz}{(r^2+z^2)^{3/2}} - \frac{\mathbf{F}_\mathrm{d}}{m_\mathrm{p}}\cdot\hat{\mathbf{e}}_z \,, \end{aligned} \tag{57}$$

where for small particles, we use the Epstein drag force expression

$$\frac{\mathbf{F}_\mathrm{d}}{m_\mathrm{p}} = \frac{\rho}{\rho_\mathrm{s}}\frac{c}{s}(r'\hat{\mathbf{e}}_r + (r\theta' - v_\mathrm{g})\hat{\mathbf{e}}_\theta + z'\hat{\mathbf{e}}_z) \,, \tag{58}$$

and for very large particles, we use the Stokes drag force

$$\frac{\mathbf{F}_\mathrm{d}}{m_\mathrm{p}} = \frac{\rho}{\rho_\mathrm{s}}\frac{C(Re)}{s}\sqrt{r'^2+(r\theta'-v_\mathrm{g})^2+z'^2}(r'\hat{\mathbf{e}}_r + (r\theta' - v_\mathrm{g})\hat{\mathbf{e}}_\theta + z'\hat{\mathbf{e}}_z) \,. \tag{59}$$

We normalize these expressions using $R = 1AU = 1.5\times 10^{13}$cm as unit distance, and $\Omega_\mathrm{K}^{-1}(R) = 2.0\times 10^{-7}$s as a unit time. This yields

$$\begin{aligned} \ddot{r} &= r\dot{\theta}^2 - \frac{r}{(r^2+z^2)^{3/2}} - \mu(r,z)\dot{r} \,, \\ \ddot{\theta} &= -2\frac{\dot{r}}{r}\dot{\theta} - \mu(r,z)\left(\dot{\theta} - \frac{v_\mathrm{g}(r,z)}{rv_\mathrm{K}(R)}\right) \,, \\ \ddot{z} &= -\frac{z}{(r^2+z^2)^{3/2}} - \mu(r,z)\dot{z} \,, \end{aligned} \tag{60}$$

where $v_\mathrm{K}(R)$ is the linear azimuthal Keplerian velocity at $R = 1AU$ and where in the Epstein regime,

$$\mu_\mathrm{E}(r,z) = \frac{\rho(r,z)}{\rho_\mathrm{s}}\frac{c(r,z)}{s\Omega_\mathrm{K}(R)} \,, \tag{61}$$

and in the Stokes regime

$$\mu_\mathrm{S}(r,z) = \frac{\rho(r,z)}{\rho_\mathrm{s}}C(Re)\frac{R}{s} \,. \tag{62}$$

The numerical integration the particles' trajectories in this model is performed using a fourth order Range-Kutta integrator.

The quantities related to the disk structure (as the gas density ρ, the gas velocity v_g and the sound speed c) are derived from the protoplanetary nebula model of Supulver & Lin (2000). In this model, the gas follows a polytropic equation of state with

$$p = K\rho^2 \text{ and } c = \sqrt{\gamma K\rho} \,, \tag{63}$$

where p is the gas pressure, with $K = 6.9\times 10^{20}$ dyn cm^4 g^{-2}, $\gamma = 1.4$ for an ideal diatomic gas (composed of pure molecular hydrogen for example) and

$$\rho(r,z) = 8.5\times 10^{-12}\left(\frac{r}{6}\right)^{-3/4}\left(1 - z^2/H^2(r)\right) \text{ g cm}^{-3} \,, \tag{64}$$

where r is in AU and $H^2(r) = 34\times 10^{-12}K(r/6)^{-3/4}\Omega_\mathrm{K}(r)^{-2}R^{-2}$ is the square of the disk scale height (in the dimensionless units). Finally, the dimensionless gas velocity is

$$\begin{aligned} \frac{v_\mathrm{g}(r)}{v_\mathrm{K}(R)} &= \frac{v_\mathrm{K}(r)}{v_\mathrm{K}(R)} + \frac{1}{2\rho}\frac{\partial\rho}{\partial r}\frac{1}{v_\mathrm{K}(R)\Omega_\mathrm{K}(r)} \\ &= r^{-1/2} - \frac{8.5\times 10^{-12}KR}{GM}\frac{3}{4}6^{3/4}r^{-1/4} = r^{-1/2} - \epsilon r^{-1/4} \,, \end{aligned} \tag{65}$$

if we ignore the variation of the gas density scale height with radius. This expression defines ϵ uniquely; with the numerical values of K, G, given above and using $M = 2\times 10^{33}g$ we have $\epsilon = 1.8\times 10^{-3}$. This expression describes how gas pressure reduces the effective gravity on the gas; this results in the slightly sub-Keplerian character of the gas velocity as found in equation (66).

5.2. *Numerical integration: particles trajectories*

5.2.1. *Small particles*

Figure 2 shows the trajectories of small particles (0.1mm to 1m) released at 1AU from height 0.01 AU, as calculated numerically using the procedure described in Section 5.1. It compares the results to those obtained analytically assuming separation of variables and constant μ which are summarized in equation (7). The analytical fit is indistinguishable from the complete numerical solution, despite these approximations.

5.2.2. *Large particles*

Figure 3 shows the numerically integrated orbit of a 10m sized particle in a protoplanetary nebula, when released from rest at radius 1AU and height 0.01 above the mid-plane. It compares the numerical results to the theoretical predictions given by equation (43), and here again, despite the approximations, the analytical fit is excellent. Note that integration for much longer times (about 1000 orbits) reveals a small but growing discrepancy in the amplitude of the oscillation. This is due to the mis-representation of the analytical expression for the amplitude of the drag force compared to its true value (see equations (27) and (28)). This discrepancy is discussed in more detail later.

5.3. *Numerical integration: Boltzmann averaging and collective behavior*

In this section, we now follow the evolution of a collection of 10,000 uniformly sized particles, in the Epstein regime (of size 1mm) and in the Stokes regime (with size 10m). We release all particles from a small interval in radius, for $0.9 < r < 1.1$. The initial radial positions are uniformly distributed in that interval. Other initial conditions depend on the regime studied, in order to be best able to perform the adequate comparisons between theory and numerical experiment. After a time t, the particles positions and velocities are gathered, and binned into regular intervals in radius and in height. The total number of particles,

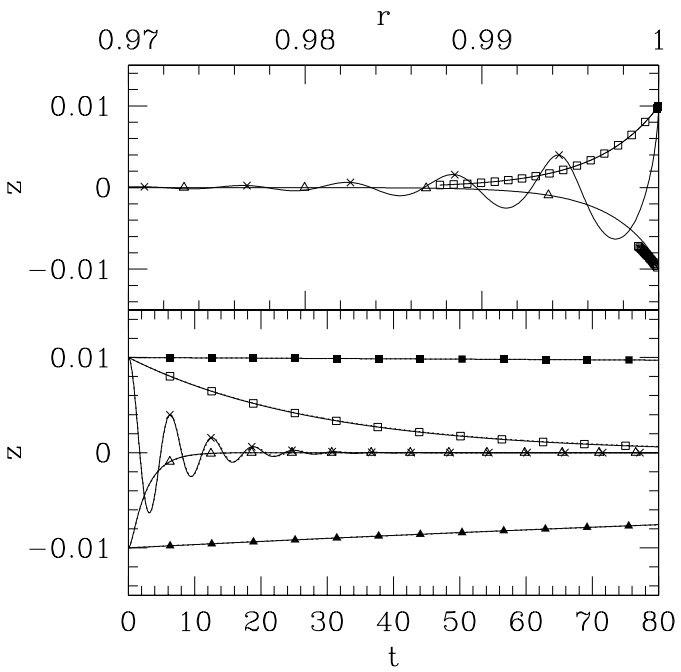

FIG. 2.— *Top figure*: trajectories of small particles in the (r,z) plane, released from radius 1 AU and heights $z = \pm 0.01$ AU successively above and below the mid-plane (to avoid crowding in the figure). The markers mimic a Pointcarré map, i.e. are positioned at the points where the particle crosses the $\theta = 0$ plane. Particles sizes are respectively: ■ = 0.1mm, ▲ = 1mm, □ = 1cm, △ = 10cm, × = 1m. *Bottom figure*: trajectories of the same particles in the (z,t) plane, with the same points-style coding for the particle sizes; again, the points represent positions of intersection with the $\theta = 0$ plane. The analytical trajectories as given by equation (7), using simply the value of μ at the position the particle, are shown as dotted lines: they are virtually indistinguishable from the numerically integrated trajectories.

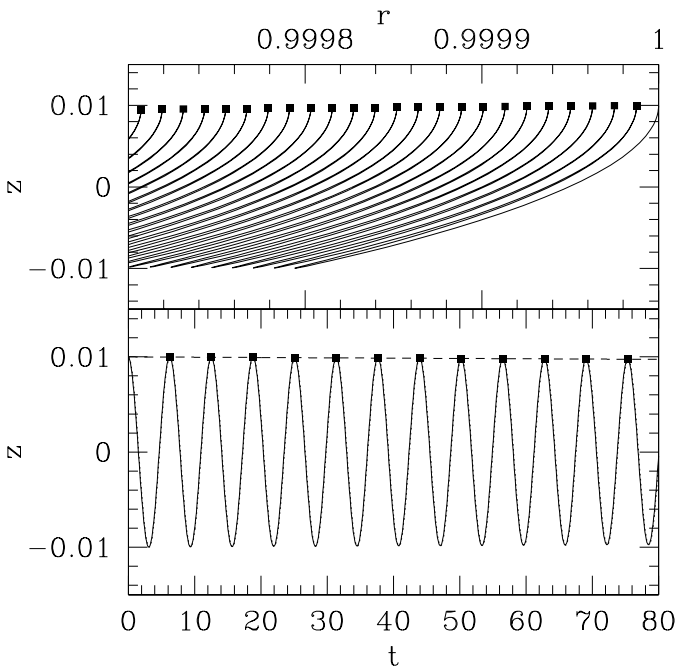

FIG. 3.— *Top figure*: trajectory of a 10 m particle in the (r,z) plane, released from radius 1 AU and height $z = 0.01$ AU above the mid-plane (to avoid crowding in the figure). The markers mimic a Pointcarré map, i.e. are positioned at the points where the particle crosses the $\theta = 0$ plane. *Bottom figure*: trajectory of the same particle in the (z,t) plane; again, the points represent positions of intersection with the $\theta = 0$ plane. The analytical trajectory as given by equation (43), using simply an average value of μ in that region ($\mu_S = 0.08$) is shown as dotted lines: they are virtually indistinguishable from the numerically integrated trajectories. Note that one must take into account the fact that the normalization of the time-variable varies with radius in the simple analytical model. The dashed line represents the envelope of the oscillation as given by equation (42).

the average velocity and the average second velocity moment are then calculated for each bin according to the formulae:

$$\rho_{\rm p}(r,z) = m_p N(r,z)\ ,$$
$$\overline{w}(r,z) = \sum_p w_p/N(r,z)\ ,$$
$$\overline{ww}(r,z) = \sum_p w_p^2/N(r,z)\ , \qquad (66)$$

where the sums are carried out over all particles found within the individual bin centered on the position (r,z).

When comparing the numerical data to the analytical solutions of the previous sections, we are careful to apply the correct normalization to the analytical formulae: indeed the normalization of the time variable depends on radial position in the analytical solutions, whereas in the numerical computations, it is normalized to the orbital frequency at 1AU.

5.3.1. *Epstein regime*

Using the normalizations adequate to the numerical calculations, the theoretical solutions for the average particle velocity and dispersion becomes

$$\overline{w} = -\frac{zr^{-3/2}}{\mu(r)} + O(\exp(-\mu(r)r^{3/2}t)\ ,$$
$$\sigma^2 \propto O(\exp(-2\mu(r)r^{3/2}t)\ . \qquad (67)$$

Figure 4 shows the very short time evolution of a collection of 10,000 mm-size particles released with a uniform distribution in heights in the interval $[-0.01, 0.01]$ AU and a uniform distribution in velocities with $-1.d-3 < w_i < 1.d-3$ (in units of the Keplerian velocity at $r = 1$). For this figure, the binning in the averaging process is fairly coarse (10 bins in each direction) in order to generate adequate statistics and to visualize the results more clearly. The velocity dispersion is indeed found to decay exponentially in accordance with equation (67).

The trajectory of these particles are then followed up to time $t = 100$ (i.e. about 16 orbits) and their average velocity is computed with a finer binning (50 bins in each direction). The results are presented in Figure 5, and compared to the analytical solutions in equation (67). Once again in this regime, the analytical solutions are found to match the numerical results very precisely.

5.3.2. *Asymptotic Stokes regime*

In the asymptotic Stokes regime, particles oscillate across the mid-plane with an algebraically decaying amplitude. Theoretical analysis of the particles' trajectories and velocities shows the velocity dispersion should remain important at all times.

In order to simplify the comparison between the analytical solutions in Section 4 and the full numerical results, we begin by releasing 10,000 10m-size particles in the disk with similar initial conditions as the ones that were used in the analytical work. Though these initial conditions may seem perhaps artificial, they are the only ones that actually provided any analytical solution. We specify the initial values

$$z_i = \frac{3\pi}{K}\cos(\varphi_i)\ ,$$
$$w_i = -4\mu_0\frac{3\pi}{K^2}\cos(\varphi_i) - \frac{3\pi}{K}\sin(\varphi_i)\ , \qquad (68)$$

where φ_i is uniformly distributed in the interval $[0, 2\pi]$. The azimuthal velocity of the particles is the Keplerian velocity at the point of release. We choose these initial values in order to simulate a set of particles released with a large range of velocities and heights above the mid-plane. The gravitationally bound particles converge toward the mid-plane during the settling phase, and continue to oscillate coherently across the mid-plane with a random phase but roughly all the same slowly decaying amplitude. The simulation is then started at $t = 0$ when all the particles have an oscillation amplitude $3\pi/K$, the corresponding velocity as given by equation (68) with a random phase. In that case, using the same normalization we adopted in our the numerical simulations, we find the theoretical solutions for the velocity dispersion to be

$$\sigma^2 = \left(\frac{9\pi^2}{(4\mu(r)t+K)^2} - z^2\right) r^{-3}\ . \qquad (69)$$

Figure 6 compares the results of the numerical calculations to the theoretical solutions given by equation (69). For relatively short time after the onset of the calculation, the numerically obtained dispersion is indeed extremely well approximated by the analytical formula. However, over much longer times, a systematic shift emerges, in which the numerical values are slightly lower than the theoretical solutions. This slight overestimate of the velocity dispersion comes from the fact that the analytical solutions underestimate the total drag force by neglecting the contributions from the particles' motion in the radial and azimuthal direction. In order to verify this conjecture, another numerical experiment is carried out in which the drag force is artificially set to

$$\mathbf{F}_{\rm d} = m_{\rm p}\frac{\rho(r,z)}{\rho_{\rm s}}C(Re)\frac{R}{s}|z|(\dot{r}\hat{\mathbf{e}}_r + (r\dot{\theta}-v_{\rm g})\hat{\mathbf{e}}_\theta + \dot{z}\hat{\mathbf{e}}_z)\ . \qquad (70)$$

In that case, the contribution of the drag force in the vertical direction is exactly that used in analytical calculation. As expected, the analytical expression is now able to reproduce the experimental results much more accurately.

Having gained some experience with the Boltzmann averaging methods, and having moreover established the adequacy of the analytical approximations to the particles' trajectories in the Stokes regime, we now attempt to use the results of the numerical simulations to find the evolution of the particles' dispersion in the case where the initial conditions are chosen randomly (rather than in such a way as to allow easy analytical calculations). In the follow up numerical computation, 10,000 10m-size particles are released with a uniform initial height and vertical velocity distribution chosen in the intervals $[-0.01, 0.01]$ AU and $[-0.01, 0.01]v_{\rm K}(R)$. The azimuthal velocity of the particles is set to be the Keplerian velocity at the point of release. With these initial conditions, the initial velocity dispersion should be uniform within the dust layer.

Figure 7 shows the evolution with time of this dispersion profile at radius $r = 1$ AU, when the particles are binned in 20 intervals in radius and heights. After a brief adjustment phase (not shown in the figure), the dispersion profile seems to be well approximated by a Gaussian distribution. We attempt to match such a Gaussian profile to the numerical data points, and find that the best fit is given by

$$\Delta(t) = \frac{3\pi}{4\mu t + 3\pi/\Delta_0}\ ,$$
$$\sigma^2(z,t) = \frac{\Delta^2(t)}{2}\exp\left(-\frac{2z^2}{\Delta^2(t)}\right)\ , \qquad (71)$$

where $\Delta_0 = 0.01$. This formula was obtained from the following heuristic arguments: according to the formula for the particles' vertical motion (see equation 43), the typical vertical velocity of the particles near the mid-plane is of the order of $\Delta(t)$,

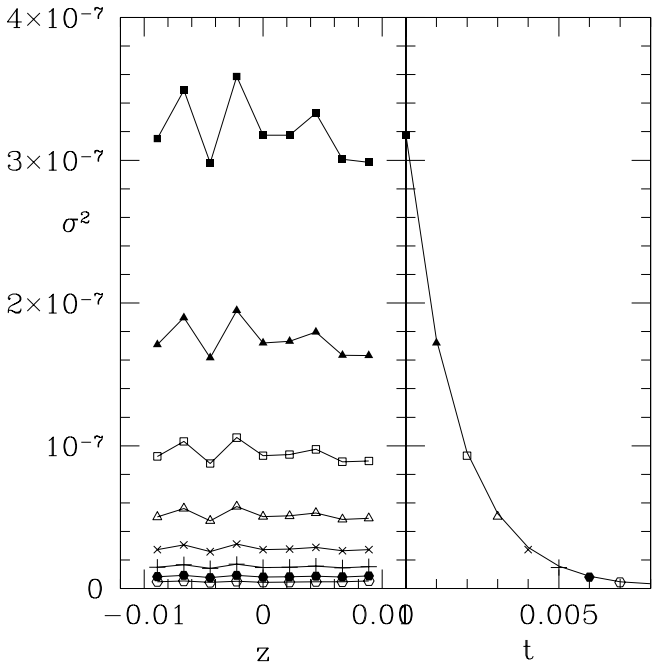

FIG. 4.— *Left figure:* Evolution of the velocity dispersion profile for a collection of mm-size particles. The style of the points used corresponds to those in the right-side figure. *Right figure* Evolution of the velocity dispersion of the particles located around $r = 1$. The points correspond to the results of the numerical experiment, and the solid line is the analytical prediction of equation (67), using a value of μ which is an average value for this quantity around $r = 1$.

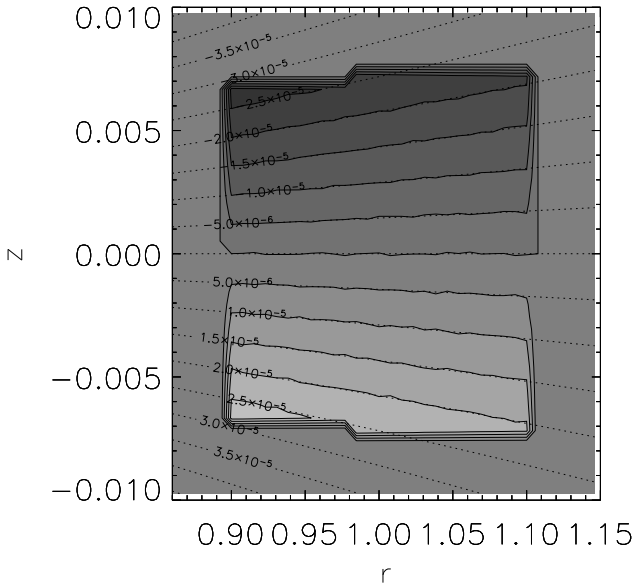

FIG. 5.— Contour plot of the average particle velocity for a collection of 10,000 mm-size particles. The solid contours as well as the gray-scale correspond to the numerical results, and the dotted lines correspond to the analytical predictions of (67), using the local value of $\mu(r,z)$ for each bin. Particles were released with a uniform distribution of heights in the interval [-0.01,0.01] AU and of radii in the interval [0.9,1.1] AU. One can easily observed the settling and (negligible) radial drift in this diagram, as well as the excellent matching between theory and this numerical experiment.

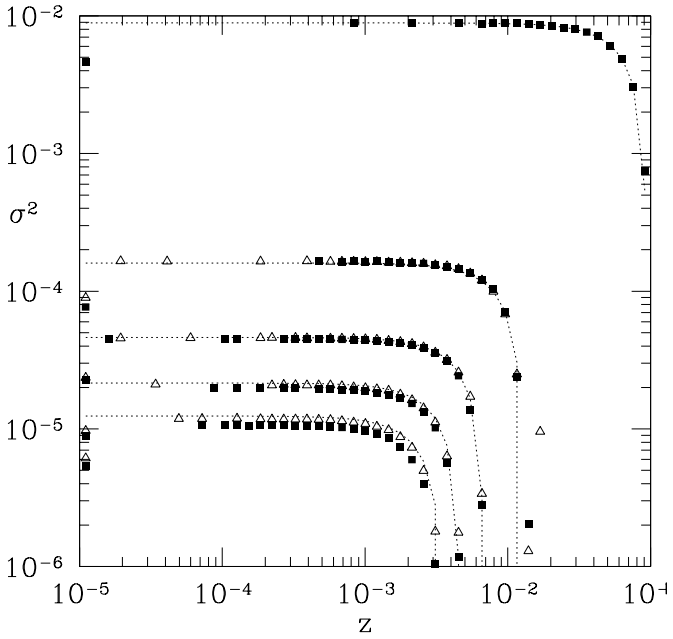

FIG. 6.— Temporal evolution of the velocity dispersion of a collection of 10m-size particles, measured at $r = 1$ AU . The successive curves (from top to bottom) correspond to times $t = 0$, $t = 2000$, $t = 4000$, $t = 6000$ and $t = 8000$ in units of the angular period at this radius. The following style coding has been used: (■) for the realistic numerical experiment and (△) for the artificially reduced drag force (as given by equation (70)). The dotted lines correspond to the analytical predictions of equation (69).

where Δ is the maximum height of the particles above the mid-plane. Moreover, Δ decays with time due to gas drag according to equation (42), so that one can readily deduce the evolution of $\Delta(t)$ for a set of particles released at $t = 0$ from typical heights ranging between 0 and Δ_0. The numerical factors have been fitted to the data. The analytical fit is also shown in Figure 7, and is found to reproduce the evolution of σ satisfactorily.

Finally, recalling that the analytical expression for the particles' vertical motion slightly underestimates the true drag force, we compare the analytical fit given by equation (71) to an artificial simulation in which the drag force is given by equation (70). In principle, the fit should be much better in this case. However, we find that the evolution of the dispersion in that case is better fitted by

$$\sigma^2(z,t) = \frac{2}{\pi}\Delta^2(t)\exp\left(-\frac{2z^2}{\Delta^2(t)}\right) , \qquad (72)$$

whilst keeping the expression for $\Delta(t)$ the same (see Figure 7). Though this difference is small, it still suggests that any attempt to find an analytical fit to the collective motion of Stokes particles should be carefully calibrated before being used in further simulations.

To conclude this Section, it was found that the analytical evaluation of one particle's orbit was extremely useful toward the determination of the collective motion of a large number of particles, and that the resulting averaged equations fit the numerical experiments extremely well. We have also been able to determine a simple heuristic way of closing the moments equations at low order in the case of particles in the Stokes regime, which emulates the effect of the particles dispersion by a mock pressure term that *can* be related to large-scale properties (and initial conditions) of the fluid.

6. EVOLUTION OF THE SIZE DISTRIBUTION OF PARTICLES IN A GASEOUS DISK

Having discussed the time-evolution of a large number of particles of equal size, we now consider a population of different-size particles. Again, the Boltzmann approach proves useful and simple to use. Let us assume for simplicity that for a given size, and at a given radius, the *initial* particles to gas mass ratio is independent of z. Hence the initial distribution of particles of a given size s at time $t = 0$ is

$$\rho_i(s,z) = \rho_0(s)\exp(-z^2/2H^2) , \qquad (73)$$

where H is the typical gas disk height; for an isothermal disk, $H = c/r\Omega_K$. Let us also assume (again for simplicity) that the initial vertical velocity of particles is null. This idealized *ad hoc* setup could correspond to a condensation front where, at time $t = 0$, both hydrogen and heavy elemental gas diffuses into a cool region of the disk. The condensation and sublimation time scales are generally much shorter than the dynamical time scales (Supulver & Lin 2000) so that, at least the small grains may form with a similar density distribution as the gas and without any initial in-falling motion. The coexistence of large and small particles well above the mid plane requires runaway coagulation of initially steady, microscopic dust grains into grains up to a size s. This rapid *in situ* growth is possible in regions where the particles have large surface density and much greater than unity area filling factor because the particles' collision and growth time scales are short compared with their dynamical time scale. The particles then start settling from their initial positions, and interact with the gas mostly with an Epstein drag law.

The particles density distribution at time t is then simply:

$$\rho_p(s,z,t) = \frac{1}{\alpha}\rho_i(z/\alpha) = \rho_0(s)\exp(-z^2/2\Delta^2)\exp(t/\mu(s)) , \quad (74)$$

where α is defined by equation (9), and $\Delta = H\alpha = H\exp(-t/\mu(s))$ is the evolving dust layer thickness. This equation was derived from (17) using the ansatz (73) and $g(w_i,z_i) =$

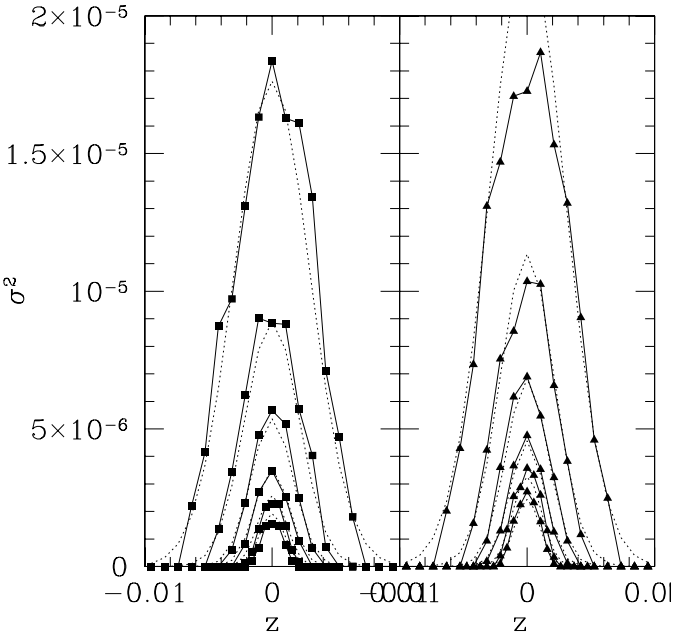

FIG. 7.— *Left panel:* Temporal evolution of the dispersion profile for a set of 10,000 10m-size particles released with a uniform spatial distribution and a uniform vertical velocity distribution. The various sets of points joined by a solid line correspond to times t = 2000, t = 4000, t = 6000, t = 8000, t = 10000 and t = 12000 (from the top-curve to the bottom curve). The initial velocity dispersion profile is not shown in order to preserve a readable scale on this plot. But it is approximately uniform in the dust layer as expected . The dotted lines are the corresponding analytical fits to the dispersion profile as given by equation (71). *Right panel:* Temporal evolution of the dispersion profile for a set of 10,000 10m-size particles released with a uniform spatial distribution and a uniform vertical velocity distribution, with the artificial drag force amplitude given by equation (70). The curves are plotted at the same time-intervals as in the left-side panel. The analytical fit, as prescribed by equation (72), is shown in dotted lines.

$\delta(w_i)$. We can deduce from this result the number distribution of particles of size s

$$\begin{aligned} n(s,z,t) &= n_0(s)\exp(-z^2/2\Delta^2)\exp(t/\mu(s)) \\ &= n_0(s)\exp(-z^2\exp(2ts/\kappa)/2H^2)\exp(ts/\kappa)\,, \end{aligned} \quad (75)$$

where we have defined the constant κ such that $\mu = \kappa/s$ in order to write explicitly this equation in terms of its dependence on the particle size. The initial particle size distribution function is taken to be that given by Hellyer (1970) and Mathis *et al.* (1977)

$$n_0(s) \propto s^{-3.5}\,. \quad (76)$$

At a given height above the disk, this distribution function peaks for small particle sizes (which corresponds to the initial peak in $n_0(s)$), but has another maximum, which evolves with time, at approximately

$$s = \frac{2\kappa}{t}\ln\left(\frac{H}{z}\right)\,, \quad (77)$$

regardless of the initial size distribution function of the particles. This result is illustrated in Fig. 9.

These results shown in Figures 8 and 9 suggest the following comments. Firstly, at a given height, successive fronts of particles with decreasing sizes pass through the gas as they settle, to leave the region completely depleted of the intermediate sized particles. Secondly, at a given time, there is a definite stratification of the particles in terms of their respective sizes, with the larger particles concentrating tightly around the mid-plane. Note that this method is only valid for particles with sizes up to the order of the mean-free-path of the gas. For the very large particles, the Stokes drag law must be applied. In that case, we have shown in Section 4 that the large particles only settle algebraically toward the mid-plane. As a result, although their number density is small, the large particles remain important at all times and at all heights in the disk.

This work shows that after a few settling times (which are of the order of a few thousands of orbits for cm-sized particles), the bulk of the disk will be depleted of intermediate sized particles, which have all settled down to the mid-plane. There remains, at all heights, very small particles that have not had time to settle, and very large ones which are in a phase of oscillation around the mid-plane.

7. SUMMARY AND DISCUSSIONS

In this paper, we provide a set of analytic solutions to describe the sedimentation of dust particles due to gas drag in a protostellar accretion disk.

The main effect of the gas drag is to induce a loss of angular momentum and linear momentum for the particle, which in turn leads to orbital decay and vertical settling. Numerical integration of the particles' trajectories in a protoplanetary accretion disk is straightforward if we assume that the gas flow is laminar and occurs mostly in the azimuthal direction. However, analytical integration is also possible given a set of assumptions (which have been checked here to be reasonably well justified), including the separability of the radial and vertical motion, and locally uniform density. Accordingly, we have extracted analytical formulae for the vertical motion of particles in a disk, both in the Epstein regime (for particles with size much smaller than the mean-free-path of the gas molecules) and in the Stokes regime (for particles much larger than the mean-free-path). Comparison of these analytical expressions with the complete numerically integrated orbits shows an excellent match in both cases.

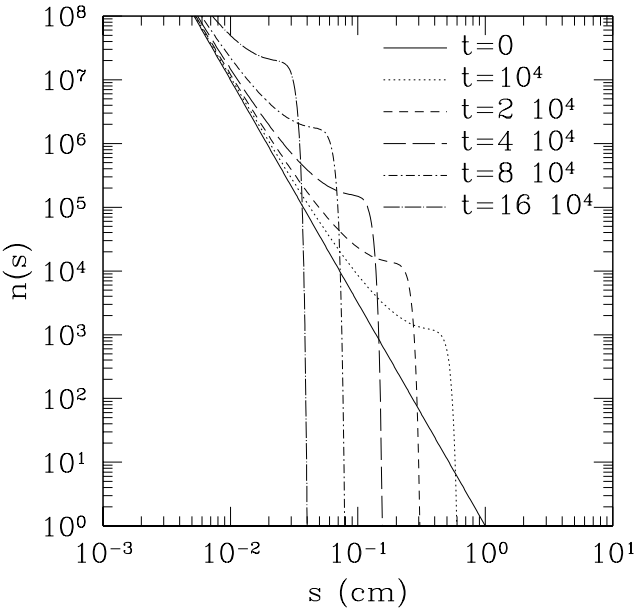

FIG. 8.— Evolution with time of the particle size distribution $n(s)$ at fixed height $z = 0.001$ (i.e. 1% of the disk scaleheight). Note how the maximum of the distribution function satisfies the relation (77).

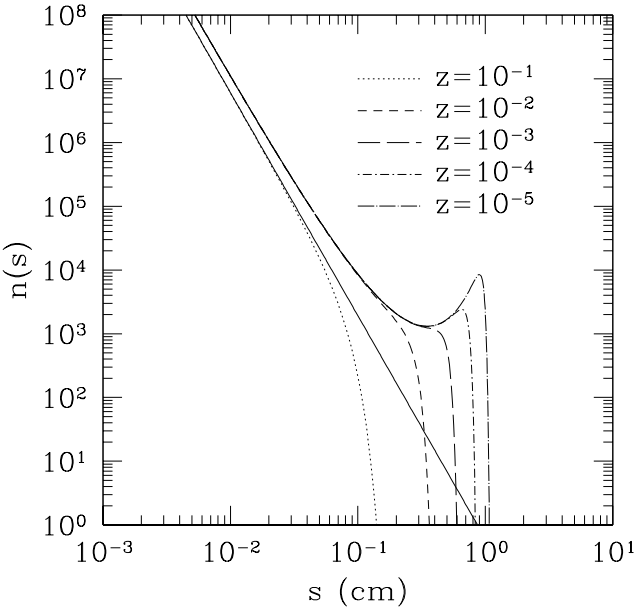

FIG. 9.— Variation with height of the particle size distribution $n(s)$ at fixed time $t = 10^4$.

By using the analytical expression for the particles' orbits, we were able to extract their average behavior using a standard Boltzmann analysis (i.e. local averaging, or rather, coarse-graining, of the particles' positions and velocities in phase space). The successive moments of the Boltzmann distribution function provide the evolution of the coarse-grained particle density, velocity and velocity dispersion. The successive moments of the Boltzmann equation yield the equivalent of "fluid" equations for the collection of particles, and in particular a mass conservation equation and a momentum equation.

Numerical experiments were performed in which 10,000 single-size particles were released in the disk from a localized region of phase-space (typically uniformly distributed in space and with a uniform vertical velocity distribution). Using a similar coarse-graining method as the one used in the analytical analysis, we were able to extract the particle density profile, their average velocity and velocity dispersion from the numerical integration. We compared them to the analytical formulae obtained previously. The main results are summarized here.

In the Epstein regime, there is an excellent agreement between the analytic formulae and the results of the numerical calculation. Individual particles have their velocity with respect to the gas quickly damped out on a very short stopping timescale. Correspondingly, their collective behavior is coherent: the typical velocity dispersion is found to decay on the particle stopping timescale, which is usually much smaller than the orbital timescale. For times longer than the stopping timescale, individual particles settle exponentially toward the mid-plane and the corresponding average momentum equation reduces to a simple standard fluid equation with a linear drag term, and null pressure.

In the Stokes regime, there is a good agreement between the theory and the results of the numerical experiments. Individual particles are found to oscillate across the mid-plane with an algebraically decaying amplitude. Although this behavior is very well reproduced by the analytical work, there exists a small discrepancy between analytical formulae and the results of numerical computation in the form of a slight systematic overestimate of the particles' oscillation amplitude. This problem is due to an (unfortunately unavoidable) over-simplification of the amplitude of the drag force in the analytical work, and results in similar discrepancies in the comparison of averaged quantities. Nonetheless, apart from this small identifiable and controllable error, the predictions of the analytical work match very well the numerical results. As expected, the particles' velocity dispersion is found to remain large at all times within the dust layer, with a maximum near the mid-plane. This large dispersion is directly related to the continuous oscillatory motion of the particles across the mid-plane. We found it extremely difficult to obtain analytical predictions of the temporal evolution of the dispersion for anything but the simplest initial conditions - which were not necessarily always realistic. However, we were able to deduce from the numerical experiments a heuristic fit to the observed evolution of the particles dispersion, for more general initial conditions. This result has interesting consequences with respect to the possibility of closing the moments equations at low order, and describing accordingly the evolution of a collection of large particles with averaged fluid equations. We will test this theory in future work.

Finally, by combining the average evolution equations for single-size particles obtained in the Epstein regime to a plausible size-distribution function for dust-grains in the ISM (Hellyer, 1970, Mathis *et al.*, 1977), we showed that it is possible to follow analytically the spatial and temporal evolution of such a size-distribution as the particles settle toward the mid-plane. This analytical calculation was done for collisionless particles, and the extension of this work to include collisions, coagulation and sublimation would probably require numerical analysis. Nonetheless, within this approximation we found that the sedimentation process results in a very strong segregation of particles according to their sizes, within a timescale of a few hundreds of years only. All intermediate-size particles quickly converge to the mid-plane, leaving behind only the very small particles, indirectly supported against the settling by gas pressure, and the very large particles, which keep oscillating across the mid-plane with a slowly decaying amplitude. This segregation process may well suggest that within the very thin dust layer at the mid-plane, one could approximate the population of dust particles by a single-size population.

In future work, we shall apply the results obtained here to two essential purposes:

- the description of the particles as a continuum fluid will be used to study the stability of the dust layer against shearing (Garaud *et al.*, in preparation), in order to test whether gravitational instability can indeed take place in the dust layer. More generally, we intend to implement this description into existing 3D HydroDynamics codes for the computation of accretion disks, in order to obtain a fully self-consistent description of dust evolution and growth in these disks;

- the temporal and spation evolution of the size-distribution of particles can be compared directly with observations of dust. We plan to construct models with which we can infer the extent of particle coagulation and infer the surface density distribution of the gas from high resolution, multi-wavelength (mostly in the sub-mm and mm range) maps of protostellar disks.

ACKNOLEDGEMENTS

Pascale Garaud thanks New Hall (Cambridge) and PPARC for financial support towards the completion of this work. It was also supported in part by NASA through grant NAG5-10612 and the California Space Institute. The authors thank Neil Balmforth and Taku Takeuchi for many useful discussions.

APPENDIX: DERIVATION OF THE PROPERTIES OF RADIAL MOTION OF PARTICLES IN A GASEOUS DISK

Neglecting the vertical motion of the particles, the equations of motion in the radial and azimuthal directions in the Epstein regime are

$$\ddot{r} - r\dot{\theta}^2 = -\frac{GM}{r^2} - \frac{c}{s}\frac{\rho}{\rho_s}\dot{r}\,, \tag{78}$$

$$r\ddot{\theta} + 2\dot{r}\dot{\theta} = -\frac{c}{s}\frac{\rho}{\rho_s}\left(r\dot{\theta} - v_g(r)\right)\,, \tag{79}$$

where $v_g(r)$ is the slightly sub-Keplerian azimuthal velocity of the gas

$$v_g(r) = \sqrt{\frac{GM}{r}} + \frac{1}{2}\sqrt{\frac{r^3}{GM}}\frac{1}{\rho}\frac{\partial p}{\partial r} = v_k(r) - \frac{\eta(r)}{\Omega_K(r)}\,, \tag{80}$$

which defines $\eta(r) = -(1/2\rho)\partial p/\partial r$. As in Section 2.3, we use the normalizations $[r] = R = 1$ and $[t] = \Omega_K^{-1}(R)$ to obtain

$$\ddot{r} - r\dot{\theta}^2 = -\frac{1}{r^2} - \mu\dot{r} \,, \tag{81}$$

$$r\ddot{\theta} + 2\dot{r}\dot{\theta} = -\mu\left(r\dot{\theta} - \frac{1}{r^{1/2}} + \frac{\eta(r)}{\Omega_K^2(r)}\right) \,. \tag{82}$$

It is not possible to find simple analytical solutions of the full system. However, we can assume that deviations from Keplerian motions are small, and that the particle velocity can be written as

$$r = 1 + \epsilon \text{ and } \dot{\theta} = 1 + \dot{\phi} \,. \tag{83}$$

The linearized system yields (assuming that the background quantities vary very little with r)

$$\ddot{\epsilon} + \mu\dot{\epsilon} - 3\epsilon = 2\dot{\phi} \,, \tag{84}$$

$$\ddot{\phi} + \mu\dot{\phi} = -2\dot{\epsilon} - \frac{3}{2}\mu\epsilon - \mu\frac{\eta}{\Omega_K^2} \,. \tag{85}$$

Substituting the first into the second yields

$$\frac{1}{2}\dddot{\epsilon} + \mu\ddot{\epsilon} + \frac{1}{2}(1+\mu^2)\dot{\epsilon} = -\mu\frac{\eta}{\Omega_K^2} \,, \tag{86}$$

hence the local solution is

$$\dot{\epsilon} = e^{-\mu t}(a\cos 2t + b\sin 2t) - 2\frac{\mu}{1+\mu^2}\frac{\eta}{\Omega_K^2} \,. \tag{87}$$

This solution represents the local difference between the particle velocity and the Keplerian velocity, in units of the Keplerian velocity. As in the solution found in Section 4, the first term represents a very quick stopping of the particle on timescale $1/\mu$ and the second term represents a constant inward drift. The variation of this drift velocity with particle size is given by the function $\mu/(1+\mu^2)$ which has a maximum for $\mu = 1$. This result reproduces the results found by Weidenschilling (1977).

REFERENCES

Adachi I., Hayashi C., Nakazawa K., 1976, Prog. Theor. Phys., 56, 1756
Adams, F. C., Lada, C. J., Shu, F. H. 1987, ApJ, 312, 788
Balbus, S. A, Hawley, J. F., 1990, ApJ, 376, 214
Beckwith, S.V.W. 1999, in *The Origin of Stars and Planetary System*, eds C.J. Lada and N.D. Kylafis, Kluwer Academic, 579
Boltzmann, L., 1872, Wien Berichten, 66, 275
Clarke, C. J., Gendrin, A., & Sotomayor, M. 2001, MNRAS, 328, 485
D'Alessio, P., Calvet, N., & Hartmann, L. 2001, ApJ, 553, 321
Goldreich P., Ward W. R., 1973, ApJ, 183, 1051
Haisch, K. E. Jr., Lada, E. A. & Lada, C. J. 2001, ApJ, 553, 153
Hellyer B., 1970, MNRAS, 148, 383
Hayashi, C. Nagazawa, K., Nagagawa, Y. 1985, in *Protostars and planets II*, eds D. Black and M. Mathews, U Arizona Press, 1100
Klahr, H. H., Lin, D. N. C., 2001, ApJ, 554, 1095
Laplace, P.S. de 1796, *Exposition du système du monde*, Paris
Marcy, G. W., Cochran, W. D., & Mayor, M. 2000, in Protostars and Planets IV, ed V. Mannings, A. P. Boss, & S. S. Russell (Tucson: Univ. of Arizona Press), 1285
Mathis J. S., Rumpl W., Nordsieck K. H., 1977, ApJ, 217, 425
Pollack, J.B., Hubickyj, O., Bodenheimer, P., Lissauer, J.J., Podolak, M., & Greenzweig, Y. 1996, Icarus, 124, 62
Prosser, C. F., Stauffer, J. R., Hartmann, L., Soderblom, D. R., Jones, B. F., Werner, M. W., McCaughrean, M. J. 1994, ApJ, 421, 517
Sekiya, M., 1998, Icarus, 133, 298
Shuping, R. Y., Bally, J., Morris, M. & Throop, H. 2003, ApJ587, 109
Supulver K. D., Lin D. N. C., 2000, Icarus 146, 525
Takeuchi, T, Artymowicz, P., 2001, ApJ, 557, 990
Takeuchi, T., Lin, D. N. C., 2002, ApJ, 581, 1344
Thi, W.F., Pontoppidan, K. M., Van Dishoeck, E.F., Dartois, E. & d'Hendecourt, L. 2002, A & A, 394, 27
Throop, H. B., Bally, J., Esposito, L. W., McCaughrean, M. J. 2001, Science, 292, 1686
Weidenschilling S. J., 1977, MNRAS, 180, 57
Weidenschilling, S.J. 1984, Icarus, 60,553
Weidenschilling S. J., Cuzzi, J. N., 1993, *Protostars & Planets III*, 1031
Wyatt, M. C., Dermott, S. F., Telesco, C. M., Fisher, R. S., Grogan, K., Holmes, E. K., Pina, R. K. 1999, ApJ, 527 918
Whipple F. L., 1972,*From plasma to planet*, ed. A. Elvius, Wiley, London
Youdin, A. N, Shu, F. H., 2002, ApJ, 580, 494
Zuckerman, B., Forveille, T., & Kastner, J. H. 1995, Nature, 373, 494